

Improved sensitivity to fluorescence for cancer detection in wide-field image-guided neurosurgery

Michael Jermyn,^{1,2,*} Yoann Gosselin,² Pablo A. Valdes,³ Mira Sibai,⁴ Kolbein Kolste,⁵
Jeanne Mercier,² Leticia Angulo,² David W. Roberts,⁶ Keith D. Paulsen,⁵
Kevin Petrecca,¹ Olivier Daigle,⁷ Brian C. Wilson,⁴ and Frederic Leblond^{2,8}

¹Brain Tumour Research Centre, Montreal Neurological Institute and Hospital, Dept. Neurology and Neurosurgery, McGill University, 3801 University St., Montreal, QC, H3A 2B4, Canada

²Dept. Engineering Physics, Polytechnique Montreal, CP 6079, Succ. Centre-Ville, Montreal, QC, H3C 3A7, Canada

³Dept. Neurosurgery, Harvard Medical School, Brigham and Women's Hospital, 75 Francis Street, Boston, MA 02115, USA

⁴Dept. Medical Biophysics, University of Toronto/University Health Network, Toronto, ON, M5G 1L7, Canada

⁵Thayer School of Engineering, Dartmouth College, 14 Engineering Drive, Hanover, NH 03755, USA

⁶Dept. Neurosurgery, Dartmouth Hitchcock Medical Center, One Medical Center Drive, Lebanon, NH 03756, USA

⁷Nuvu cameras, 5155 Decelles avenue, Pavillon JA Bombardier, Montreal, QC, H3T 2B1, Canada

⁸Centre de Recherche du Centre Hospitalier de l'Université de Montréal, rue Saint-Denis, Que, H2X 0A9, Canada

*Michael.Jermyn@mail.mcgill.ca

Abstract: In glioma surgery, Protoporphyrin IX (PpIX) fluorescence may identify residual tumor that could be resected while minimizing damage to normal brain. We demonstrate that improved sensitivity for wide-field spectroscopic fluorescence imaging is achieved with minimal disruption to the neurosurgical workflow using an electron-multiplying charge-coupled device (EMCCD) relative to a state-of-the-art CMOS system. In phantom experiments the EMCCD system can detect at least two orders-of-magnitude lower PpIX. *Ex vivo* tissue imaging on a rat glioma model demonstrates improved fluorescence contrast compared with neurosurgical fluorescence microscope technology, and the fluorescence detection is confirmed with measurements from a clinically-validated spectroscopic probe. Greater PpIX sensitivity in wide-field fluorescence imaging may improve the residual tumor detection during surgery with consequent impact on survival.

©2015 Optical Society of America

OCIS codes: (170.3890) Medical optics instrumentation; (170.6280) Spectroscopy, fluorescence and luminescence.

References and links

1. C. Nimsky, A. Fujita, O. Ganslandt, B. Von Keller, and R. Fahlbusch, "Volumetric assessment of glioma removal by intraoperative high-field magnetic resonance imaging," *Neurosurgery* **55**(2), 358–371 (2004).
2. Q. T. Nguyen and R. Y. Tsien, "Fluorescence-guided surgery with live molecular navigation—a new cutting edge," *Nat. Rev. Cancer* **13**(9), 653–662 (2013).
3. W. Stummer, U. Pichlmeier, T. Meinel, O. D. Wiestler, F. Zanella, and H.-J. Reulen; ALA-Glioma Study Group, "Fluorescence-guided surgery with 5-aminolevulinic acid for resection of malignant glioma: a randomised controlled multicentre phase III trial," *Lancet Oncol.* **7**(5), 392–401 (2006).
4. W. Stummer, H. Stepp, G. Möller, A. Ehrhardt, M. Leonhard, and H. J. Reulen, "Technical principles for protoporphyrin-IX-fluorescence guided microsurgical resection of malignant glioma tissue," *Acta Neurochir. (Wien)* **140**(10), 995–1000 (1998).
5. G. Widhalm, S. Wolfsberger, G. Minchev, A. Woehrer, M. Krssak, T. Czech, D. Prayer, S. Asenbaum, J. A. Hainfellner, and E. Knosp, "5-Aminolevulinic acid is a promising marker for detection of anaplastic foci in diffusely infiltrating gliomas with nonsignificant contrast enhancement," *Cancer* **116**(6), 1545–1552 (2010).
6. P. A. Valdés, F. Leblond, A. Kim, B. T. Harris, B. C. Wilson, X. Fan, T. D. Tosteson, A. Hartov, S. Ji, K. Erkmen, N. E. Simmons, K. D. Paulsen, and D. W. Roberts, "Quantitative fluorescence in intracranial tumor: implications for ALA-induced PpIX as an intraoperative biomarker," *J. Neurosurg.* **115**(1), 11–17 (2011).

7. Y. Kajimoto, T. Kuroiwa, S. Miyatake, T. Ichioka, M. Miyashita, H. Tanaka, and M. Tsuji, "Use of 5-aminolevulinic acid in fluorescence-guided resection of meningioma with high risk of recurrence," *J. Neurosurg.* **106**(6), 1070–1074 (2007).
8. K. Bekelis, P. A. Valdés, K. Erkmen, F. Leblond, A. Kim, B. C. Wilson, B. T. Harris, K. D. Paulsen, and D. W. Roberts, "Quantitative and qualitative 5-aminolevulinic acid-induced protoporphyrin IX fluorescence in skull base meningiomas," *Neurosurg. Focus* **30**(5), E8 (2011).
9. P. Valdes, F. Leblond, and V. L. Jacobs, "Fluorescence detection in the operating room: a review of principles, methods, and applications," *Curr. Med. Imaging Rev.* **8**, 211–232 (2012).
10. P. A. Valdés, V. Jacobs, B. T. Harris, B. C. Wilson, F. Leblond, K. D. Paulsen, and D. W. Roberts, "Quantitative fluorescence using 5-aminolevulinic acid-induced protoporphyrin IX biomarker as a surgical adjunct in low-grade glioma surgery," *J. Neurosurg.* **123**(3), 771–780 (2015).
11. D. N. Louis, H. Ohgaki, O. D. Wiestler, W. K. Cavenee, P. C. Burger, A. Jouvett, B. W. Scheithauer, and P. Kleihues, "The 2007 WHO Classification of Tumours of the Central Nervous System," *Acta Neuropathol.* **114**(2), 97–109 (2007).
12. M. Lacroix, D. Abi-Said, D. R. Fournay, Z. L. Gokaslan, W. Shi, F. DeMonte, F. F. Lang, I. E. McCutcheon, S. J. Hassenbusch, E. Holland, K. Hess, C. Michael, D. Miller, and R. Sawaya, "A multivariate analysis of 416 patients with glioblastoma multiforme: prognosis, extent of resection, and survival," *J. Neurosurg.* **95**(2), 190–198 (2001).
13. W. Stummer, H.-J. Reulen, T. Meinel, U. Pichlmeier, W. Schumacher, J.-C. Tonn, V. Rohde, F. Oettel, B. Turowski, C. Woiciechowsky, K. Franz, and T. Pietsch; ALA-Glioma Study Group, "Extent of resection and survival in glioblastoma multiforme: identification of and adjustment for bias," *Neurosurgery* **62**(3), 564–576 (2008).
14. K. Petrecca, M.-C. Guiot, V. Panet-Raymond, and L. Souhami, "Failure pattern following complete resection plus radiotherapy and temozolomide is at the resection margin in patients with glioblastoma," *J. Neurooncol.* **111**(1), 19–23 (2013).
15. M. J. McGirt, K. L. Chaichana, F. J. Attenello, J. D. Weingart, K. Than, P. C. Burger, A. Olivi, H. Brem, and A. Quinones-Hinojosa, "Extent of surgical resection is independently associated with survival in patients with hemispheric infiltrating low-grade gliomas," *Neurosurgery* **63**(4), 700–708 (2008).
16. M. S. Berger, A. V. Deliganis, J. Dobbins, and G. E. Keles, "The effect of extent of resection on recurrence in patients with low grade cerebral hemisphere gliomas," *Cancer* **74**(6), 1784–1791 (1994).
17. G. E. Keles, K. R. Lamborn, and M. S. Berger, "Low-grade hemispheric gliomas in adults: a critical review of extent of resection as a factor influencing outcome," *J. Neurosurg.* **95**(5), 735–745 (2001).
18. T. Hollon, S. L. Hervey-Jumper, O. Sagher, and D. A. Orringer, "Advances in the Surgical Management of Low-Grade Glioma," *Semin. Radiat. Oncol.* **25**(3), 181–188 (2015).
19. A. Kim, M. Khurana, Y. Moriyama, and B. C. Wilson, "Quantification of in vivo fluorescence decoupled from the effects of tissue optical properties using fiber-optic spectroscopy measurements," *J. Biomed. Opt.* **15**(6), 067006 (2010).
20. P. A. Valdés, F. Leblond, V. L. Jacobs, B. C. Wilson, K. D. Paulsen, and D. W. Roberts, "Quantitative, spectrally-resolved intraoperative fluorescence imaging," *Sci. Rep.* **2**, 798 (2012).
21. P. A. Valdes, V. L. Jacobs, B. C. Wilson, F. Leblond, D. W. Roberts, and K. D. Paulsen, "System and methods for wide-field quantitative fluorescence imaging during neurosurgery," *Opt. Lett.* **38**(15), 2786–2788 (2013).
22. X. Zhang, "Instrumentation in Diffuse Optical Imaging," *Photonics* **1**(1), 9–32 (2014).
23. J. Hernandez-Palacios and L. L. Randeberg, "Intercomparison of EMCCD- and sCMOS-based imaging spectrometers for biomedical applications in low-light conditions," in (2012), Vol. 8215, p. 82150Q–82150Q–9.
24. C. A. Combs, "Fluorescence microscopy: a concise guide to current imaging methods," *Curr. Protoc. Neurosci.* Editor. Board Jacqueline N Crawley **AI Chapter 2**, Unit2.1 (2010).
25. C. Li, G. S. Mitchell, J. Dutta, S. Ahn, R. M. Leahy, and S. R. Cherry, "A three-dimensional multispectral fluorescence optical tomography imaging system for small animals based on a conical mirror design," *Opt. Express* **17**(9), 7571–7585 (2009).
26. F. Bestvater, Z. Seghiri, M. S. Kang, N. Gröner, J. Y. Lee, K.-B. Im, and M. Wachsmuth, "EMCCD-based spectrally resolved fluorescence correlation spectroscopy," *Opt. Express* **18**(23), 23818–23828 (2010).
27. M. Burkhardt and P. Schwille, "Electron multiplying CCD based detection for spatially resolved fluorescence correlation spectroscopy," *Opt. Express* **14**(12), 5013–5020 (2006).
28. O. Daigle, C. Carignan, J.-L. Gach, C. Guillaume, S. Lessard, C.-A. Fortin, and S. Blais-Ouellette, "Extreme faint flux imaging with an EMCCD," *Publ. Astron. Soc. Pac.* **121**(882), 866–884 (2009).
29. P. A. Valdés, A. Kim, F. Leblond, O. M. Conde, B. T. Harris, K. D. Paulsen, B. C. Wilson, and D. W. Roberts, "Combined fluorescence and reflectance spectroscopy for in vivo quantification of cancer biomarkers in low- and high-grade glioma surgery," *J. Biomed. Opt.* **16**(11), 116007 (2011).
30. P. A. Valdés, F. Leblond, A. Kim, B. C. Wilson, K. D. Paulsen, and D. W. Roberts, "A spectrally constrained dual-band normalization technique for protoporphyrin IX quantification in fluorescence-guided surgery," *Opt. Lett.* **37**(11), 1817–1819 (2012).
31. C. Poynton, *Digital Video and HDTV* (Morgan Kaufmann, 2003), pp. 291–292.
32. N. Sanai, L. A. Snyder, N. J. Honea, S. W. Coons, J. M. Eschbacher, K. A. Smith, and R. F. Spetzler, "Intraoperative confocal microscopy in the visualization of 5-aminolevulinic acid fluorescence in low-grade gliomas," *J. Neurosurg.* **115**(4), 740–748 (2011).

33. K. Roessler, A. Becherer, M. Donat, M. Cejna, and I. Zachenhofer, "Intraoperative tissue fluorescence using 5-aminolevulinic acid (5-ALA) is more sensitive than contrast MRI or amino acid positron emission tomography ((18)F-FET PET) in glioblastoma surgery," *Neurol. Res.* **34**(3), 314–317 (2012).
-

1. Introduction

The goal of neurosurgery in brain tumor management is to maximize the extent of tumor resection while minimizing functional impairment secondary to surgery. Standard surgical equipment comprises a white-light neurosurgical microscope and a neuronavigation unit to guide surgery based on preoperative magnetic resonance imaging (MRI). The use of preoperative MRI improves the accuracy and safety of surgical resections using spatial co-registration of MRI scans with intraoperative magnified bright-field images taken in real time during surgery. Indeed, image-guided neurosurgery has increased the completeness of tumor resection as determined by comparing tumor tissue visible in preoperative relative to postoperative MRI [1].

More recently, intraoperative fluorescence imaging based on the optical contrast of molecules such as indocyanine green, fluorescein and protoporphyrin IX (PpIX) has emerged [2]. PpIX is synthesized and retained preferentially in tumor cells following administration of the pro-drug 5-aminolevulinic acid (ALA). The biological origin of the optical contrast varies between fluorophores, each providing different and potentially complementary clinical information. For example, preferential accumulation of PpIX in tumor cells results in part from differences in heme biosynthesis and pro-drug uptake. Glioblastoma resection surgery guided by the red fluorescence of PpIX upon violet light excitation has been demonstrated in controlled clinical trials to improve the completeness of tumor resection relative to resections based solely on bright-field, white-light visualization [3].

For the majority of clinical studies of ALA-PpIX guided resection of brain tumors, fluorescence detection is achieved with a commercial neurosurgical microscope [4]. The emitted fluorescence is detected by a color RGB camera or by the naked eye through the oculars of the microscope. The resection is thus guided by subjective visual assessment of the fluorescence images in real time, referred to as qualitative fluorescence imaging.

Clinical reports have suggested that the metabolic marker PpIX aids in surgical guidance of other brain pathologies, including meningioma and metastatic brain lesions [5–8]. It has also been used in other organs for tumor localization and treatment guidance [9]. However, qualitative fluorescence imaging is intrinsically limited in sensitivity and specificity. The *sensitivity*, i.e. the ability to detect (residual) tumor, is hampered by the limited detection efficiency of CCD cameras (e.g., read-out noise, quantum efficiency), the presence of the leakage reflectance signals into the detection path (background), and the confounding effects of intrinsic tissue optical properties [6]. Specificity is negatively impacted by the lack of spectral resolution when using high-pass interference filtering. Importantly, this limitation prevents subtraction of tissue auto-fluorescence background, which places a lower limit on the concentration of the exogenous fluorophore that can be detected and does not allow simultaneous imaging of multiple fluorophores. Moreover, studies using point fluorescence measurements combined with diffuse reflectance spectroscopy suggest that low-grade gliomas also produce diagnostic levels of ALA-induced PpIX but that the signals are too low to be detected with standard qualitative wide-field fluorescence imaging [6,10]. Patients with glioblastomas (WHO grade 4 gliomas [11]) do see some survival benefits based on maximizing extent of resection [12,13] and complete resection is a major factor in preventing recurrence and improving survival for grade 4 gliomas [14]. Although the specificity of PpIX uptake in glioblastomas can inhibit the ability to maximize extent of resection, particularly in areas of edema, providing more sensitive fluorescence imaging can give the surgeon additional information to make more informed decisions during surgery. Completeness of resection for low-grade gliomas can considerably extend survival and potentially be curative

[15–17], motivating the need to improve current fluorescence imaging during brain (and other) tumor resections [18].

We have previously reported techniques and instruments to circumvent some of the limitations of qualitative fluorescence imaging. We developed a contact fiberoptic probe combining fluorescence and diffuse reflectance spectroscopy, allowing for the correction of light attenuation by the tissue on fluorescence signal and giving absolute PpIX tissue concentration [19,20]. With a contact fiberoptic probe, we have detected PpIX concentrations as low as ~ 1 ng/ml in brain tissue phantoms under violet light excitation and in clinical *in vivo* clinical measurements have shown ALA-PpIX accumulation in low-grade glioma as low as ~ 1 – 10 ng/ml [6,19]. Building upon this work, we then developed a modular, wide-field spectroscopic imaging system using a scientific CMOS (sCMOS) camera integrated onto an optical port of a commercial fluorescence neurosurgical microscope [21]. In other work, we used a CCD-based system for glioblastoma resection in patients, demonstrating that it is able to detect brain tumor margins beyond what can be detected with qualitative fluorescence imaging coupled with neuronavigation and MRI [20]. However, when compared with the contact fiberoptic point probe system, the sensitivity of the both the CMOS and CCD systems is at least 10 to 20 times less, due primarily to the camera read-out noise [21], compromising the ability to detect the low levels of ALA-PpIX often present in low-grade gliomas. An electron-multiplying charge-couple device (EMCCD) allows for fast, high performance signal detection, particularly for low exposure times or in low-light conditions [22–24], and has seen use in spectrally resolved fluorescence tomography [25] and fluorescence correlation spectroscopy [26,27]. In this report we demonstrate that wide-field spectroscopic detection of PpIX using the state-of-the-art sCMOS system can be further improved with an EMCCD imaging detector, and that this technology can also be seamlessly integrated into the neurosurgical workflow.

2. Methods

2.1. System setup

The new fluorescence system is shown in Fig. 1 and consists of custom optical adapters, the same LCTF as used in the sCMOS system, a coherent fiber-optic imaging bundle (Schott) and an hNü EMCCD camera (Nüvü Camēras). The custom adapters couple the imaging bundle, LCTF and camera to an optical port on a commercial neurosurgical microscope (BLUE 400 Pentero, Carl Zeiss Meditec) equipped with a blue light source and fluorescence detection capabilities.

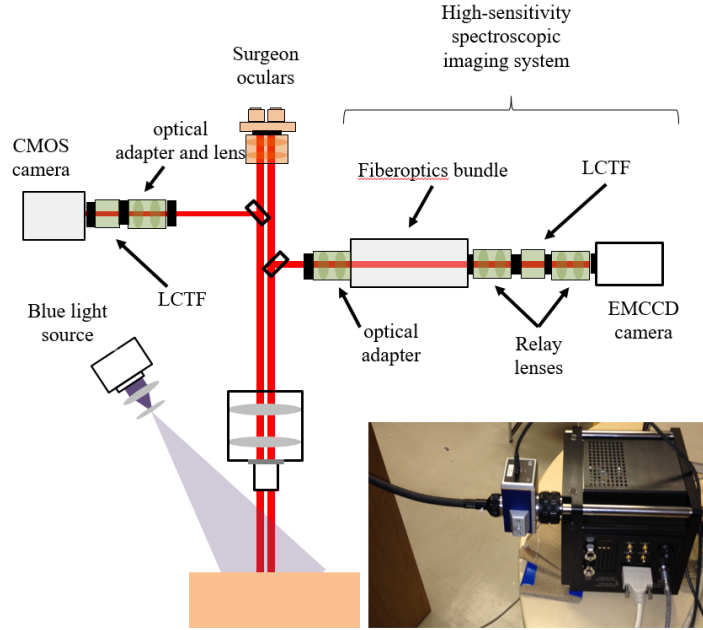


Fig. 1. Schematic of the imaging set up used to evaluate the performance of the EMCCD- and CMOS-based spectral imaging systems connected to different ports on a commercial neurosurgical microscope. The photograph shows the EMCCD system, including the coherent imaging bundle used for remote light detection.

An imaging bundle is required, because the size ($15.5 \times 15.5 \times 17.8$ cm) and weight (4.5 kg) of the EMCCD camera prevents it from being directly mounted to the microscope's optical port. The 91 cm long bundle comprises a square array (1.6 cm^2) of 400×400 optical fibers each of $60 \text{ }\mu\text{m}$ core diameter. The LCTF performs single-band filtering ($\sim 7 \text{ nm}$ full-width at half maximum) in the visible range (400-720 nm) and has a wavelength-dependent transmittance (maximum 64% at 710 nm and out-of-band rejection $\sim 4 \text{ OD}$). The EMCCD camera has 512×512 pixels, 92% peak quantum efficiency (QE), effective read-out noise of $< 0.1 e^-$ at 20 MHz, and a thermal noise $D = 0.0002 e^-/\text{pixel/s}$ at its lowest cooling temperature of -85°C . Custom LabView software (National Instruments, Austin, TX) controls data acquisition, processing and image display. The amplification gain on the EMCCD camera can be set to values as high as $G = 5000$ but, unlike the sCMOS system, is affected by an $F = \sqrt{2}$ excess noise factor induced by the stochastic processes in the electron multiplying register and by a charge injection noise of $C < 0.001 e^-/\text{pixel}$. The EMCCD signal-to-noise ratio (SNR) is given by [28]

$$SNR = \frac{QE \times (I^{PpIX} + I^{Bkg})}{\sqrt{F^2 [(I^{PpIX} + I^{Bkg}) \times QE \times T + D \times T + C] + \frac{\sigma^2}{G^2}}}, \quad (1)$$

The same formula applies for the sCMOS camera, and all parameters for both systems are described in Table 1. For the EMCCD system, the dominant sources of noise are charge injection noise and to a lesser extent thermal noise. For the sCMOS system, the dominant sources of noise are readout noise and thermal noise.

Table 1. Descriptions of the parameters used in Eq. (1), with the relevant values for the EMCCD and sCMOS systems.

Parameter	Description	EMCCD value	sCMOS value
QE	Quantum efficiency at peak	92%	60%
F	Excess noise factor induced by the stochastic process in the electron multiplying register	$\sqrt{2}$	1
T	Image integration time	(varies)	(varies)
D	Thermal noise	0.0002 e ⁻ /pixel/s	0.08 e ⁻ /pixel/s
C	Charge injection noise	< 0.001 e ⁻ /pixel	0
σ	Readout noise	100 e ⁻ /pixel	1.5 e ⁻ /pixel
G	Amplification gain	Up to 5000	1
I^{PpIX}	Fluorescence signal from PpIX	-	-
I^{Bkg}	Non-specific contributions to the signal: autofluorescence and ambient	-	-
$(I^{PpIX} + I^{Bkg}) \times QE$	Signal	-	-
$\sqrt{(I^{PpIX} + I^{Bkg}) \times QE}$	Shot noise	-	-

2.2. Phantom study

We devised an experimental protocol to compare quantitatively the sensitivity of the EMCCD- and sCMOS-based systems under identical conditions. As illustrated in Fig. 1, the systems were simultaneously connected to equivalent optical ports of the neurosurgical microscope. A power meter was used to verify that the fraction of signal sent to both optical ports is equal, using the same magnification. The violet light source integrated into the microscope illuminated tissue-simulating liquid phantoms containing different PpIX concentrations. The phantoms also contained a lipoprotein suspension (Intralipid) to provide brain tissue-like scattering coefficients at the excitation wavelength ($\mu_s' = 15\text{-}25 \text{ cm}^{-1}$ @ 405 nm) and yellow food coloring (McCormick) as the optical absorber ($\mu_a = 20\text{-}60 \text{ cm}^{-1}$ @ 405 nm) [29]. Nine sets of phantoms of different absorption-scattering combinations were prepared, each combination being used with 5 different PpIX concentrations: 5 and 1 $\mu\text{g/ml}$ and 200, 40 and 8 ng/ml. The optical coefficients at the emission wavelength (600 nm) ranged from $\mu_a = 0.02$ to 0.06 cm^{-1} and $\mu_s' = 8.7$ to 14.5 cm^{-1} . Fluorescence images were acquired simultaneously for each phantom with both cameras for integration times (per wavelength) of $T = 5, 10, 20, 40,$ and 80 ms. 11 images were acquired from 400 to 430 nm and 41 images from 600 to 720 nm with 3 nm spectral resolution, for a total of 52 images. The incident excitation light power density was $\sim 5 \text{ mWcm}^{-2}$ over a circular field of view of 20 cm^2 at a distance of 30 cm between the microscope condenser lens and the phantom surface. Spectroscopic reflectance images were also acquired under white-light illumination. Quantitative fluorescence values were computed using previously-reported algorithms [20,30] in which the raw fluorescence spectra are normalized with the reflectance spectra to account for the spectral distortion caused by tissue absorption and scattering. Spectral un-mixing was used to separate the contribution of PpIX from background signal including intrinsic fluorescence, using a nonnegative least-squares approach [19,20]. As described previously [20,30], a calibration factor was determined from a PpIX dilution experiment that related the attenuation-corrected spectra to actual dye concentrations. This procedure produced an estimate of PpIX concentration at the tissue surface (in $\mu\text{g/ml}$) for each image pixel.

2.3. Ex vivo tissue study

To test the utility of performing fluorescence imaging enabled by the EMCCD, two female Lewis rats (Charles River, QC, Canada) were used under institutional approval (University Health Network, Toronto, Canada). For tumor induction, the rats were placed under 4% isoflurane anesthesia (oxygen flow at 2 L/min), induced in a chamber and sustained by 1-

2.5% isoflurane at 1 L/min via a rat-adapted nose cone. The eyes were lubricated with tear gel, and the animals were placed on a warming blanket. For each rat, the scalp was shaved and disinfected with betadine and isopropanol, followed by a 1.5 cm incision along the midline. A 1 mm burr hole was made in the left hemisphere, 3 mm posterior to the bregma and 2 mm to the left of the sagittal suture, exposing the dura but leaving it intact. Subsurface intracranial brain tumors were induced by injection of 10^5 RG2 (ATCC CRL-2433) cells in 5 μ L of RPMI-1640 media (Sigma-Aldrich) through the burr hole, at a depth of 2 mm below the dura using a 26G Hamilton syringe. Tumors were allowed to grow for 14 days to a size of 3-4 mm. On the day of surgery, 120 mg/kg of ALA (Sigma-Aldrich) was injected intraperitoneally. Four hours post-injection, each rat was sacrificed; the whole brain was removed intact and sectioned into 3-4 mm thick slices under subdued light. The brain sections were mounted on a tissue cassette and were then frozen in liquid nitrogen/isopentane.

On the day of imaging, the tissue samples were slowly thawed to room temperature. For each of the 7 tissue samples (3 from one animal and 4 from the other), a sequence of spectroscopic fluorescence and diffuse reflectance images were acquired using the EMCCD from 400 to 430 nm and 600-720 nm with 3 nm spectral resolution. Fluorescence and white-light images were also acquired using the clinical Zeiss Pentero surgical microscope equipped with a 400 nm excitation fluorescence imaging option. The exposure time with the EMCCD varied from 10 to 100 ms with a gain of 500. Background images were also taken with no excitation light. Each sample lying on one side of the tissue cassette was placed at the same position in a box made to isolate the sample from ambient light sources. The sample was retained in the cassette to keep it intact. The fluorescence spectra were normalized using the reflectance spectra to account for the effects of tissue absorption and scattering, and spectral un-mixing was applied to separate the contribution of the fluorophore from background signals including tissue autofluorescence, based on the acquired background images with no excitation light [19,20]. A hand-held optical probe was used to measure fluorescence in the tissue slices. The probe, described previously [19,29], has optical fibers for fluorescence excitation at 405 nm, and spectroscopic detection between 430 and 750 nm. The diffuse reflectance spectra at two different source-detector fiber separations is also measured and used to derive the tissue absorption and scattering properties that are then applied to the measured fluorescence spectrum to derive the absolute fluorophore concentration in the tissue. For each slice, the probe was placed in contact with the tissue specimen to measure fluorescence at a single location. The measurement locations for the probe were chosen as positions with high fluorescence observed on the standard qualitative fluorescence image.

3. Results

3.1. Phantom study

Figure 2 shows the fluorescence imaging estimates of PpIX concentration as a function of the true values in the phantoms for the two systems using different exposure times. The calibration factor allows the x and y axis to be expressed in the same units (μ g/ml), while the attenuation correction factor brings the data points closer together along the y -axis [30].

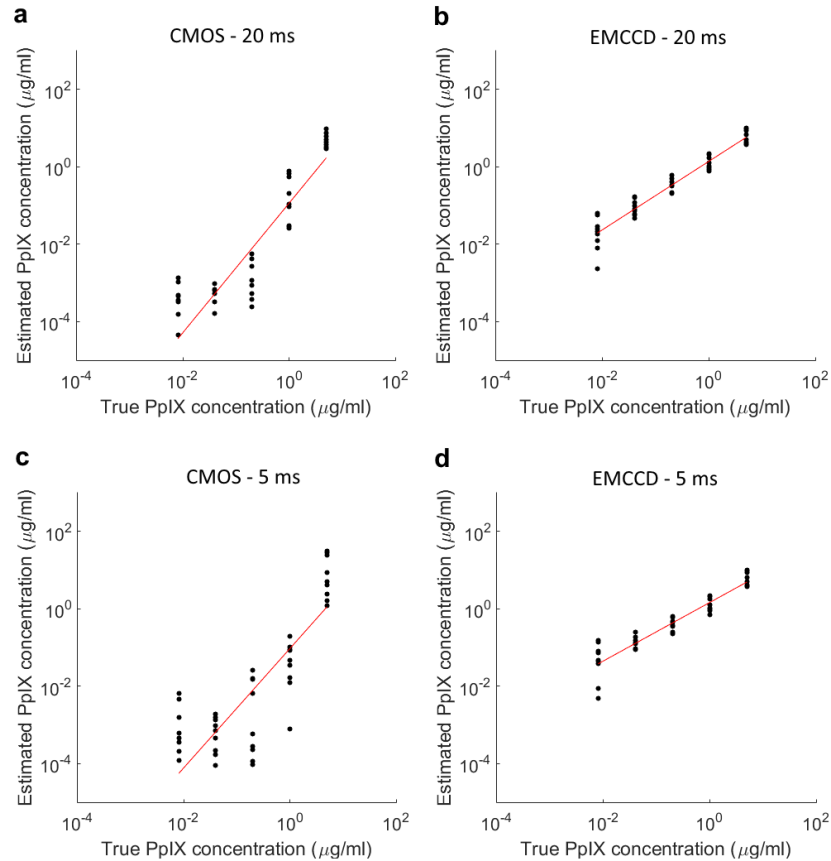


Fig. 2. Recovered values of PpIX concentration *versus* the known PpIX values in the different tissue-simulating phantoms for both the CMOS (a,c) and EMCCD systems (b,d) with integration times of 5 ms per wavelength (a,b) and 20 ms per wavelength (c,d). Measurements were averaged over a 5 by 5 pixel window in the center of the inclusion. Measurements at each PpIX concentration correspond to 9 phantoms with different absorption-scattering combinations at 600 nm ranging from $\mu_a = 0.02$ to 0.06 cm^{-1} and $\mu_s = 8.7$ to 14.5 cm^{-1} . The lines of fit are in red.

These plots indicate that the quantified fluorescence varies linearly with concentration to the lowest PpIX level (8 ng/ml) for the EMCCD system, but the linearity breaks down at around 40 ng/ml for the sCMOS system at a 20 ms exposure time (no significant linearity observed for a 5 ms exposure time, see below for discussion of the linearity at different exposure times). Thus, since the noise floor of the EMCCD system was not reached at the lowest concentration, its sensitivity is at least 1-2 orders of magnitude greater than that of the sCMOS system, which is the current state-of-the-art for ALA-PpIX fluorescence detection in neurosurgical guidance. In fact, the sensitivity is comparable to that of the point probe that has a PpIX detection limit $\sim 1 \text{ ng/ml}$. The R^2 values for the fit of estimated vs. true PpIX concentration, for the CMOS and EMCCD systems and for each exposure time, are listed in Table 2. These quantities were computed based on the residuals for the linear fit of all points for a particular exposure time (i.e. the values for all phantoms at all concentrations for one exposure time yield a single R^2 value). The R^2 values for the EMCCD system are 0.89 or greater for all exposure times, while those for the CMOS system range from 0.64 to 0.79 for exposure times less than 40 ms, demonstrating the improved sensitivity of the EMCCD system for fluorescence detection, particularly at lower fluorophore concentrations and for

lower exposure times. The R^2 value for an 80 ms exposure time is somewhat greater for the CMOS system.

Table 2. R^2 values for the fit of quantified PpIX concentration (log) vs true PpIX concentration (log) for the CMOS and EMCCD systems at different exposure times.

Exposure time (ms)	R^2 for CMOS quantification (a.u.)	R^2 for EMCCD quantification (a.u.)
5	0.64	0.89
10	0.69	0.91
20	0.79	0.93
40	0.92	0.93
80	0.95	0.92

Limitations of the sCMOS system sensitivity are further illustrated in the spectra of Fig. 3, in which the 635 nm PpIX emission peak cannot be detected even at 40 ng/ml concentration for 20 ms exposure time. The PpIX emission peak is not visible with the CMOS system for exposure times of 5, 10 and 40 ms (data not shown), whereas the peak is visible for all exposure times with the EMCCD system. The increased EMCCD system sensitivity is directly related to its multiplication gain that, as shown in Eq. (1), attenuates the read-out noise.

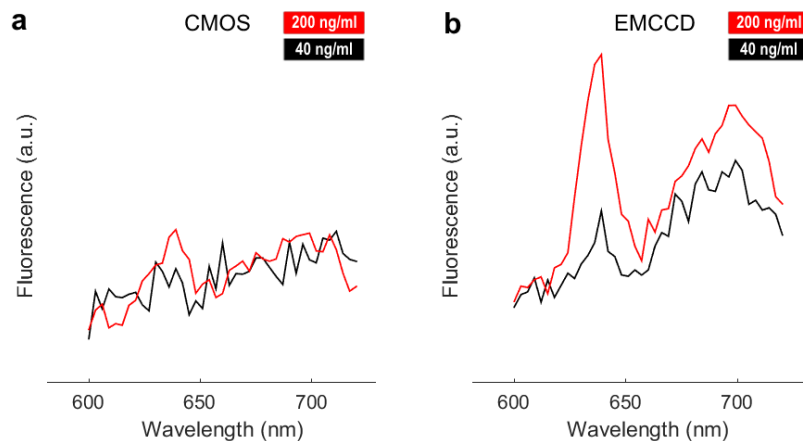


Fig. 3. Examples of fluorescence spectra acquired with both imaging systems for 20 ms exposure at PpIX concentrations of 40 and 200 ng/ml and with optical properties $\mu_a = 0.03 \text{ cm}^{-1}$ and $\mu_s = 14.5 \text{ cm}^{-1}$. The measurements were averaged over a 5 by 5 pixel window at the center of the inclusion, and the spectra are normalized by reflectance data.

The results presented here suggest that the excess noise factor, F , and the injection charge noise, C , do not meaningfully affect the EMCCD's detection sensitivity under experimental conditions relevant to its intended clinical use. However, larger values of C , as found in other EMCCD camera models, could negatively impact performance for PpIX detection.

3.2. *Ex vivo tissue study*

Figure 4 shows images of tissue samples acquired using the surgical microscope's internal RGB camera (TRIO 630 integrated camera system for the Pentero microscope) and the fluorescence images acquired with the EMCCD system. In each sample, two areas identified by boxes 1 and 2, compare the recovered contrast of the EMCCD system with the visible contrast attained through the qualitative fluorescence imaging feature available on the Pentero microscope. Contrast ratio (CR) was calculated as the ratio of intensity in box 1 or 2 to the intensity in the background box shown in Fig. 4. The background box was selected as an area of tissue where negligible fluorescence was observed.

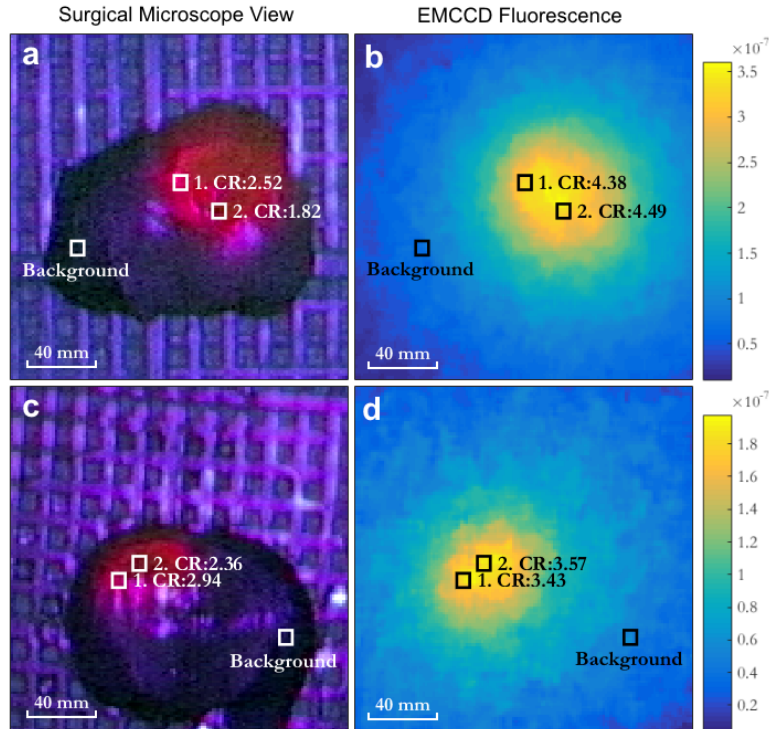


Fig. 4. (a,c) Two *ex vivo* brain tissue samples containing glioma, as viewed through the neurosurgical microscope under violet light excitation. (b,d) show the corresponding images for the derived quantitative fluorescence using the EMCCD system. Representative contrast ratios (CR) are shown within the tumor. The images have been cropped to highlight the tissue samples.

For the EMCCD, the intensity represents the recovered fluorescence value (as described in *Materials and Methods*). For the microscope, the intensity I_m from the surgical microscope's internal RGB camera was calculated as the luminance [31] in order to represent the visibility of each color component in the fluorescent image:

$$I_m = \frac{299R + 587G + 114B}{1000} \quad (2)$$

where red (R), green (G) and blue (B) correspond to the intensity values of the corresponding color components in the broadband image. Luminance was used in order to quantify the visual contrast observed by the human eye in the RGB image from the surgical microscope, since it is the current standard used by neurosurgeons for assessing the presence of fluorescence. It may be possible to optimize a camera setup for better contrast detection of fluorescence by selecting appropriate spectral detection bands, however the RGB camera used is from a commercial neurosurgical microscope for fluorescence-guided surgery, and so this represents the standard for comparison. For both tissue samples, the EMCCD fluorescence results in greater contrast ratios than the visible fluorescence obtained through the neurosurgical microscope in areas of high (box 1 in both images) as well as less visible fluorescence (box 2 in both images). The fiberoptic contact probe was used to measure a single location on each tissue sample corresponding to a location of high visible fluorescence on the microscope image, and the measured fluorescence from the probe was compared with the fluorescence recovered in a 5 by 5 pixel window at the same location in the EMCCD image (Fig. 5).

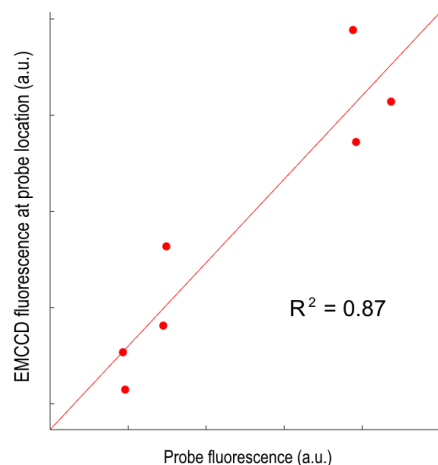


Fig. 5. Correlation between the quantitative PpIX fluorescence measured with the EMCCD system at 7 different locations (averaged over 5 by 5 pixel regions) and the corresponding quantitative point probe measurements. The linear regression line is also shown.

There is good correlation between the EMCCD and probe data ($R^2 = 0.87$), which allows the EMCCD thresholds in Section 3.A to be compared directly with the detection capabilities of the probe. The probe can detect PpIX concentrations as low as 1 ng/ml *in vivo*. Hence, since the EMCCD system (i) can detect as little as 8 ng/ml PpIX in phantoms, (ii) demonstrates linearity in fluorescence quantification for a range of concentrations and optical properties for exposure times as low as 5 ms, and (iii) shows strong correlation with the probe for fluorescence detection, indicating its detection capabilities are comparable to the highly sensitive point probe system, the clinical value of which has already been proven in high and low-grade glioma surgery [29].

4. Discussion

We have demonstrated that a spectroscopic EMCCD-based imaging system out-performs the state-of-the-art sCMOS-based imaging system currently used in ALA-PpIX fluorescence-guided tumor resection. Its higher detection sensitivity translates directly into an ability to detect substantially lower ALA-PpIX concentrations. As demonstrated in clinical studies to date, reliable detection of lower fluorophore concentrations should translate into improved completeness of tumor resection, particularly in quantitative fluorescence imaging mode where the confounding effects of variable light attenuation by the tissue are minimized [6,20,32,33]. The increase in wide-field detection sensitivity can be achieved despite the added light losses (estimated ~30%) from the imaging bundle between the camera and the microscope. The presence of non-specific signals from tissue autofluorescence and ambient light can limit the benefits associated with the enhanced sensitivity provided by EMCCD detection during surgical interventions. However, ambient light is minimized during fluorescence-guided surgeries and our clinical measurements with the probe system to date indicate that the autofluorescence intensity is considerably smaller than the PpIX emissions associated with gliomas [29]. Furthermore, the *ex vivo* tissue results demonstrate that the EMCCD system has improved fluorescence detection sensitivity under these conditions.

Perhaps the most important finding in the phantom study is that wide-field fluorescence quantification can potentially achieve a level of sensitivity comparable to that obtained with a state-of-the-art quantitative point contact probe that is currently being used to guide glioma resection in clinical trials [20]. The lowest concentrations of PpIX (8 ng/ml) detected here are consistent with the concentrations found in low-grade gliomas using a clinically-validated

quantitative fluorescence-reflectance fiberoptic probe [6,10]. This indicates that the level of improved sensitivity for the EMCCD system is relevant for low-grade glioma surgery, especially since the noise floor of the system has not yet been reached at these concentrations. The EMCCD-based system performance will be tested in future studies in patients undergoing ALA-induced fluorescence-guided glioma resection. The ability to generate wide-field images with the same level of disease detection sensitivity as currently achievable only in point-by-point mode is an important advantage in clinical practice.

Acknowledgments

This work was supported by the Canadian Foundation for Innovation (CFI), the Discovery Grant program from the Natural Sciences and Engineering Research Council of Canada (NSERC) and the Industrial Innovation and Scholarships program (partnered NSERC, Fonds de recherche du Québec - Nature et technologies – FRQNT and Nüvü Camēras). Additional support was provided by the US National Institutes of Health (R01 NS052274), Banque Nationale, Groupe de Recherche en Sciences et Technologies biomédicales (GRSTB), a Norris Cotton Cancer Center Prouty grant and a Hitchcock Foundation Pilot Project grant.